CHARACTERIZATION OF SUPERPARAMAGNETIC IRON OXIDE NANOPARTICLES WITH DIFFERENT SURFACTANTS - IN SEARCH OF OPTIMUM SYNTHESIS PARAMETERS FOR MRI APPLICATION

OSAMA AHMAD SALAMEH ABU NOQTA

UNIVERSITI SAINS MALAYSIA
2018

CHARACTERIZATION OF SUPERPARAMAGNETIC IRON OXIDE NANOPARTICLES WITH DIFFERENT SURFACTANTS - IN SEARCH OF OPTIMUM SYNTHESIS PARAMETERS FOR MRI APPLICATION

By

OSAMA AHMAD SALAMEH ABU NOQTA

Thesis submitted in fulfilment of the requirements
for the degree of
Doctor of Philosophy

December 2018

ACKNOWLEDGEMENT

On this memorable day in my life, I reached the final destination of my journey as a PhD student; first of all, I would like to thank Almighty Allah for granting me health and patience to complete this research work.

Also, I am deeply thankful to my main supervisor, **Professor Dr. Azlan Abdul Aziz,** for his support, kind cooperation, useful contribution and valuable guidance throughout the course of this study. Thanks again Prof. for having your door open every time I needed help.

I thank Dr. Katsikini Maria of Department Solid State, School of Physics, Aristotle University of Thessaloniki, Greece, for her great contribution and suggestion in my experiments have proved to be extremely valuable. I express appreciation to the staff of the Nano-Optoelectronics Research and Technology Laboratory (NOR lab) and INFORMM lab assistants for technical assistance during my laboratory work, particularly in the sample characterizations.

My heartfelt gratitude also goes to my family members: to my father and mother for their continuous prayers and support. I also dedicate to my wife who is my source of strength and inspiration. Finally, I thank all who supported me in any respect during the completion of this study.

Osama Ahmad Abu Noqta

Penang-Malaysia

TABLE OF CONTENTS

LIST OF FIGURES

LIST OF TABLES

LIST OF SYMBOLS

^{o}C	Degree Celsius
Oe	Oersted (magnetizing field)
H_c	Coercivily
M_r	Remanence
M_s	Saturation magnetization
M_w	Molecular weight
r_1	Transverse Relaxation rate
r_2	Longitudinal Relaxation rate
T_1	Transverse Relaxation Time
T_2	Longitudinal Relaxation Time
Å	Angstrom
IC_{50}	The half maximal inhibitory concentration
OD_{570}	Optical density at wavelength 570 nm
nm	nanometer
µl	Microliter
θ	Angle
λ	wavelength
ω_o	Larmor frequency
ζ	Zeta potential

B_o	magnetic field
d_{hkl}	interplanar spacing
D_p	Crystal size
ε	The strain
a	Lattice constant
h,k,l	Miller indices
γ	gyromagnetic ratio
Hz	Hertz
^1H	Proton

LIST OF ABBREVIATIONS

APTES	3-aminopropyl triethoxysilane
APES	3-aminopropyl-diethy-ethoxysilane
APDES	3-aminopropyl-ethyl-diethoxysilane
P(OEGMA-co-MAA)	Oly(oligo(ethylene glycol) methacrylate -co-tert-butyl methacrylate)
CS-MNPs	Chitosan-coated magnetic iron oxide nanoparticles
EO	Ethylene oxide
VSM	Vibrating sample magnetometer
COOH	Carboxylate group
DLS	Dynamic Light Scattering
CTAB	Cetyl trimethylammonium bromide
ppm	Parts per million
FTIR	Fourier-Transform Infrared Spectroscopy
HA	Humic acids
HLB	Hydrophilic–lipophilic balanced
OH	Hydroxyl group
IONPs	Iron oxide nanoparticles
IEP	Isoelectric point
MNPs	Magnetic nanoparticles

MRI	Magnetic Resonance Imaging
nm-Fe_3O_4	Nanometer-Magnetite
NPs	Nanoparticles
W/O	Water-in-Oil
O/W	Oil-in-Water
OA-MIONs	Oleic acid coated magnetic iron oxide nanoparticles
PDl	Polydispersity Index Values
PEG	Polyethylene glycol
PVP	Polyvinylpyrrolidone
pH	Potential of Hydrogen
RF	Radio Frequency
TR	Repetition Time
TE	Echo time
SPIONs	Superparamagnetic Iron Oxide Nanoparticles
TEM	Transmission Electron Microscopy
PEI	Polyethylenimine
PVA	Poly (vinyl alcohol)
XAS	X-ray Absorption Spectroscopy
XAFS	X-ray Absorption Fine Structure
XANES	X-ray Absorption Near Edge Structure

XRD	X-ray Diffraction
FWHM	Full width at half maximum
LDA	Laser doppler anemometry
HZB	Helmholtz-Zentrum Berlin
DMSO	Dimethyl sulfoxide
FOV	Field of view
C-USPION	Citrate Coated Ultra-Small Superparamagnetic Iron Oxide Nanoparticles.
CMNPs	Magnetic nanoparticles

PENCIRIAN NANOPARTIKEL OKSIDA FERUM SUPERPARAMAGNETIK DENGAN PERBAGAI SURFAKTAN YANG BERLAINAN - MENCARI PARAMETER SINTESIS OPTIMUM UNTUK APLIKASI MRI

ABSTRAK

Nanopartikel superparamagnetik oksida ferum (SPIONs) telah dikaji secara meluas dalam aplikasi bioperubatan, seperti agen kontras pengimejan resonans magnet (MRI), dan hipertermia. Pendekatan yang paling biasa digunakan untuk menghasilkan SPIONs adalah kaedah presipitasi bersama. Walau bagaimanapun, masalah berkaitan aglomerasi dan taburan saiz nanopartikel yang pelbagai yang terhasil melalui kaedah presipitasi bersama menghalang kemajuan aplikasinya dalam MRI. Oleh yang demikian, kajian ini bertujuan untuk menghasilkan SPIONs yang lebih stabil dan ekasebar untuk agen kontras MRI. Dalam tesis ini, SPIONs disintesis dengan pelbagai surfaktan (tri-natrium sitrat, polyvinylpyrrolidone (PVP), kitosan, cetyl trimethylammonium bromide (CTAB) dan asid sitrik) menggunakan kaedah presipitasi sebekas bagi pengubahsuaian permukaan dan untuk memastikan kestabilan koloid yang cemerlang dalam air. Di samping itu, parameter sintesis seperti kepekatan surfaktan, pH, dan suhu reaksi dioptimumkan untuk mendapatkan SPIONs yang stabil. SPIONs yang disediakan bersama tri natrium sitrat membentuk SPIONs paling stabil disebabkan oleh keadaan fisiologi yang lebih baik, penyebaran dan penstabilan dalam larutan akueus. Selain itu, sitrat -SPIONs menunjukkan potensi zeta (ζ = -44.0 mV) dan pemagnetan tepu (M_s = 53.9 emu g^{-1}) tertinggi berbanding sampel lain, disebabkan oleh keupayaan tiga kumpulan karboksilat yang dipisahkan daripada sitrat untuk mengikat kuat kepada permukaan SPIONs. Pengukuran TEM dari SPIONs yang berbeza menunjukkan jenis surfaktan mempengaruhi saiz purata partikel dan taburan saiz. Di samping itu, kehadiran kecacatan dalam struktur spinel, iaitu, pengoksidaan

SPIONs, seolah-olah juga dipengaruhi oleh pilihan surfaktan. Sisihan struktur di antara pelbagai sampel SPION secara langsung mempengaruhi sifat magnet SPIONs. Parameter sintesis optimum untuk pengubahsuaian permukaan diperbaiki daripada sitrat -SPIONs diperolehi, dan ia termasuk kepekatan sitrat 25 M, pH 11 dan suhu 85 ^{o}C. Di bawah keadaan optimum ini, sitrat-SPIONs menunjukkan saiz zarah ~ 9.5 nm, taburan saiz lebih sempit, kekristalan yang tinggi bersama ketepuan pemagnetan yang tinggi (M_s = 60.9 emu g^{-1}) dan kestabilan koloid yang sangat baik. Untuk aplikasi MRI, sensitiviti sitrat -SPIONs yang dioptimumkan meningkat apabila kepekatannya dalam agar fantom meningkat dari 0 (sampel kosong) menjadi 1 mg/ml, disebabkan penurunan dalam masa relaksasi T_1 dari 3055.2 hingga 990.1 ms. Begitu juga, masa relaksasi T_2 dipendekkan dari 187.6 hingga 8.8 ms apabila kepekatan sitrat -SPION dalam agar fantom meningkat dari 0 hingga 1mg/ml. Nilai r_1 dan r_2 sitrat-SPION adalah 0.65 dan 107.49 mM^{-1} s^{-1}, masing-masing, dengan nisbah r_2/r_1 sebanyak 165.37. Di samping itu, sitrat-SPIONs menunjukkan kapasiti yang tinggi untuk mengurangkan masa relaksasi T_2 dan T_1 dengan lebih daripada, masing-masing, 95.3% dan 67.6%. Berdasarkan sensitiviti mereka, sitrat-SPIONs yang disediakan oleh kaedah presipitasi bersama yang telah diubahsuai mempunyai potensi sebagai calon agen kontras MRI.

CHARACTERIZATION OF SUPERPARAMAGNETIC IRON OXIDE NANOPARTICLES WITH DIFFERENT SURFACTANTS - IN SEARCH OF OPTIMUM SYNTHESIS PARAMETERS FOR MRI APPLICATION

ABSTRACT

Superparamagnetic iron oxide nanoparticles (SPIONs) have been extensively studied for various biomedical applications, such as magnetic resonance imaging (MRI) contrast agents, and hyperthermia. The most common approach used to produce SPIONs is co-precipitation method. However, problem due to agglomeration and the broad size distribution of nanoparticles prepared by co-precipitation method hinder their application progress in MRI. Therefore, this study aims to produce a highly stabilized and monodispersed SPIONs for MRI contrast agents. In this thesis, SPIONs were synthesized with different surfactants (tri-sodium citrate, polyvinylpyrrolidone (PVP), chitosan, cetyl trimethylammonium bromide (CTAB) and citric acid) using the one pot co-precipitation method for surface modification and to ensure excellent colloidal stability in water. In addition, the synthesis parameters such as surfactant concentration, pH, and temperature of reaction were optimized to obtain stabilized SPIONs. The SPIONs prepared in the presence of tri-sodium citrate formed the most stable SPIONs due to improved physiological condition, dispersion and stabilization in aqueous solution. In addition, citrate-SPIONs displayed the highest zeta potential (ζ= -44.0 mV) and saturation magnetization (Ms=53.9 emu g^{-1}) compared with other samples, due to the ability of three carboxylate groups dissociated from the citrate to strongly bind to the surface of SPIONs. The TEM measurements of the different SPIONs indicated that the type of surfactant affects their average particle sizes and size distribution. In addition, the presence of defects within the spinel structure, i.e., oxidation of the SPIONs, seems to be also influenced by the choice of surfactant. These

structural deviations among the various SPIONs samples directly affect the magnetic properties of the SPIONs. The optimum synthesis parameters for improved surface modification of citrate-SPIONs were obtained, and they include citrate concentration of 25 M, pH of 11 and temperature of 85 ^{o}C. Under these optimum conditions, citrate-SPIONs exhibited particle size of ~9.5 nm, narrower size distribution, high crystallinity with high saturation magnetization (Ms=60.9 emu g^{-1}) and excellent colloidal stability. For MRI application, the sensitivity of the optimized citrate-SPIONs was increased when its concentration in the agar phantom increase from 0 (blank sample) to 1mg/ml, this is due to decreased in T_1 relaxation times from 3055.2 to 990.1 ms. Similarly, the T_2 relaxation time shortened from 187.6 to 8.8 ms when the concentration of citrate-SPIONs in the agar phantom increase from 0 to 1mg/ml. The r_1 and r_2 values of citrate-SPIONs are 0.65 and 107.49 mM^{-1} s^{-1}, respectively, with r_2/r_1 ratio of 165.37. In addition, the citrate-SPIONs demonstrated a high capacity to reduce T_2 and T_1 relaxation times by more than 95.3% and 67.6%, respectively. Based on their sensitivity, citrate-SPIONs prepared by modified co-precipitation method have a potential as candidate for MRI contrast agent.

CHAPTER 1: INTRODUCTION

1.1 History of Nanotechnology

The idea of nanotechnology was initiated by a physicist named Richard Feynman in his well-known address titled ‘There’s plenty of room at the bottom’ at an assembly of the American Physical Society held in December, 1959 [1]. Nanoscience involves the study of the phenomena and exploitation of materials at nanoscale, where their properties vary considerably from those at a bulk phase [2, 3]. Currently, nanotechnology is described as the design, characterization, manufacture, and harnessing the properties of structures, devices and systems by modifying their morphologies and sizes at the nanoscale [4, 5].

Materials exhibit relatively exceptional thermal, physical, chemical and optical properties at nanoscale compared to their bulk counterpart. Due to their unique physicochemical properties, nanomaterials, especially metal oxide nanoparticles, have been used in an extensive array of applications in numerous disciplines such as electronics, optical communications and biomedical systems [6-10]. One of the most common metal oxides used in biomedical applications is iron oxide nanoparticles [11, 12].

1.2 Superparamagnetic Iron Oxide Nanoparticles (SPIONs)

Iron oxide nanoparticles (IONPs) are inorganic materials with diameters ranging from 1 to100 nm. Iron oxide displays superparamagnetic properties at particle size goes smaller than 30 nm at room temperature [13]. Superparamagnetic behaviour is an intrinsic feature of IONPs, since after the absence of the magnetic field that applies to IONPs, their magnetization will disappears, thus preventing the possible agglomeration and embolization of the capillary vessels [14, 15]. The unique

physicochemical and magnetic properties of SPIONs account for their various use in biosensing, magnetic hyperthermia, bioseparation, lateral flow assay, and magnetic resonance imaging [16].

1.3 SPION as contrast agents for magnetic resonance imaging (MRI)

The biocompatibility, low toxicity, and biodegradable *in vivo* conditions of SPIONs have enabled their use as MRI contrast agent [13]. Moreover, SPIONs exhibits a higher MRI signal contrast compared to those of Gadolinium (Gd^{3+}) and Manganese (Mn^{2+}) complexes. This relatively higher contrast of SPIONs can be attributed to their high saturation magnetization by reason of increased of the number of Fe atoms that initiate for such high saturation magnetization in SPIONs [17]. Therefore, the ability of the SPIONs to improve the sensitivity of MRI and application in multiple diagnoses has emerged.

1.4 Problem Statement

The biomedical applications of SPION are based on their chemical stability and monodisperse under physiological conditions. Several methods have been used to synthesize of SPIONs. Co-precipitation method is considered the simplest, most cost-effective technique, and requires the lowest temperature for synthesizing SPIONs. In addition, it is the most cited SPION synthesis technique. SPIONs have been synthesized in the form magnetite (Fe_3O_4) or maghemite (γ-Fe_2O_3) via the co-precipitation of Fe^{2+} and Fe^{3+} ions in the ratio of 1:2 in alkaline solution under degassed environment as demonstrated by Bee [18]. However, agglomeration and the broad size distribution of nanoparticles prepared by co-precipitation method are the main drawbacks of this method [19]. As shown in Table 1.1, the samples produced through conventional co-precipitation method display poor zeta potential values in the range

of 0 to ±30 mV. Therefore, it can be inferred that the repulsive forces in SPIONs are inadequate to prevent agglomeration and that the particles lack good colloidal stability. Due to the low zeta potential, the SPIONs produced from the co-precipitation process display less sensitivity when applied as MRI probe.

The reasons for poor colloidal stability and broad size distribution of the SPIONs synthesized by the conventional co-precipitation method can be related to the mechanism of co-precipitation. The co-precipitation process involves two stages, which are the nucleation that arises when the concentration of the species attains critical supersaturation, and the growth of the nuclei through diffusion of the solutes to the crystal surface [20, 21]. To synthesize monodispersed nanoparticles, the nucleation and growth processes should be separated; that is, nucleation should be circumvented during the growth process [22].

Table 1.1 Comparison of the colloidal stability between the SPION functionalized with different surfactants as reported in literature.

Sample Name	Particle Size (nm)	Zeta Potential (mV)	Ref.
L-Arginine @ SPION	26.0	3.8	[23]
Hexanoic acid @ SPION	----------	21.2	
PIO-3	9.0	-25.0	[24]
uncoated SPION	10.0	----------	[25]
APES@ SPION		2.50 ±0.21	
APDES@ SPION		3.45 ±0.23	
APTES @ SPION		9.36 ±0.19	
P(OEGMA-co-MAA) coated SPION	10.1	-15.0	[26]
CS-MNPs	16.0	-30.0	[27]

To overcome these limitations, the SPIONs need to be stabilized and size distribution reduced by modifying their surfaces with biocompatible materials and controlling the synthesis procedures. A more recent method combines synthesis and functionalization of SPION in the presence of a surfactant as capping agent, a technique referred to as one-pot coprecipitation [28]. For example, poly(glycerol) copolymers have been employed in the synthesis of stable iron oxide nanoparticles

[29], while Sun and Zeng used oleic acid as a surfactant to ensure the uniform size distribution of iron oxide nanoparticles [30]. Lutz et al. also used copolymers [poly-(oligo (ethylene glycol) methacrylate-co-methacrylic acid)] to functionalize the magnetic nanoparticles [26]. Si et al. utilized polyelectrolytes to produce monodisperse magnetic nanoparticles [19]. However, these studies were unable to achieve excellent colloidal stability of SPIONs [28].

Therefore, this thesis aims to produce highly stable and monodispersed SPIONs for MRI contrast agent using the proper surfactant and systematically controlling and manipulating the flow of the reacting precursors.

1.5 Objectives of Study

The main objectives of this study are as follows:

1) To study the effect of surfactants on the structural, morphology, and magnetic properties of SPIONs produced by one pot co-precipitation method.

2) To optimize the synthesis parameters of the SPIONs formation using one pot co-precipitation method.

3) To produce stable and monodisperse SPIONs through surface modification using the optimum surfactant.

4) To evaluate the sensitivity of the SPIONs prepared under optimum synthesis parameters for application as MRI probe (contrast agent).

1.6 Scope of Study

The main scope of this study is to prepare highly stable and monodispersed SPIONs in the presence of five different surfactants through one-pot co-precipitation method. This study intends to evaluate the sensitivity of SPIONs prepared under optimum synthesis parameters as a contrast agent in magnetic resonance imaging in agarose gel phantom.

1.7 Outline of Thesis

This study comprises seven chapters. The current chapter presents a historical background of nanotechnology, introduces SPIONs, and explains the application of SPION as contrast agent for MRI. The problem statement, objectives and scope of research are also covered in this chapter. Chapter Two covers the properties and phases of iron oxide as well as theoretical background of MRI and MRI contrast agents. Chapter Three provides a detailed and concise literature review of the synthesis of SPION and surface modification of SPION with different surfactants. The Fourth Chapter presents the experimental setup for one pot co-precipitation method, the characterization instruments, and preparation of citrate-SPION for application as MRI probe. The results of this study are presented in the Fifth Chapter, and they include crystalline structure, TEM images, size distribution, stability of citrate-SPION colloids in the suspensions, XAFS measurements, and magnetic properties of the as-synthesized SPIONs, which were analyzed and discussed. The optimization of surfactant concentration, pH, and temperature of SPION synthesis were also presented in Chapter Five. This Chapter also explains the sensitivity of citrate-SPIONs prepared under optimum synthesis parameters for application as MRI probe. Finally, the study was concluded and potential avenues for future research recommended in Chapter Six.

CHAPTER 2: THEORETICAL BACKGROUND

2.1 Introduction

The distinct particle size and chemical stability of iron oxide nanoparticles under different physiological conditions in addition to their specific magnetic saturation account for their extensive use in biomedicine [31]. Therefore, synthesis of such functional nanoparticles requires a very good insight into the influence of synthesis parameters (temperature, additives, surfactant concentration, type of precursor solutions, etc.) on their size, morphologies, dispersivity, crystal defects, etc. Therefore, this chapter covers the iron oxide phases and their properties. The theories, principles, mechanisms and applications of MRI and MRI contrast agents are also presented in this chapter.

2.2 Theory of iron oxide nanoparticles (IONPs)

In biomedical applications, the major problems associated with the synthesis of IONPs are agglomeration and uncontrolled particle size. The agglomeration has been attributed to high or large surface area, Van der Waals forces of cohesive attraction and dipole-dipole relations between the nanoparticles [32]. Hence, the adding of surfactants into the synthesis iron oxide nanoparticles plays a significant role in controlling their nucleation and growth, and also to prevent their agglomeration [33]. Several organic and inorganic materials, such as citric acid, chitosan, polyvinylpyrrolidone (PVP), silica and gold nanoparticles [34-38], have been used to modify the surface of IONPs and inhibit agglomeration via either electrostatic repulsion or steric stabilization.

2.2.1 Iron oxide phases

Iron oxide is a readily available, ubiquitous compound that consists of iron and oxygen atoms. It comprises sixteen iron oxide phases, which are listed in Table 2.1 [39]. Iron oxide nanoparticles can be obtained in several phases such as magnetite, hematite, maghemite and goethite, depending on the conditions of synthesis.

Table 2.1 Iron oxides and hydroxides phases [40].

Iron hydroxides and hydrous oxides		**Iron oxides**
Goethite α-FeOOH	Ferrihydrite $Fe5HO_8$	Hematite α-Fe_2O_3
Lepidocrocite $Fe(OH)_2$	Bernalite $Fe(OH)_3$	Magnetite Fe_3O_4
Akaganéite β-FeOOH	Green Rust	Maghemite γ -Fe_2O_3
Schwertmannite	Feroxyhyte δ'-FeOOH	β-Fe_2O_3
Ferrimagnetic δ-FeOOH	High pressure FeOOH	ε-Fe_2O_3
		Wustite FeO

3.2.1(a) Hematite (α-Fe_2O_3)

Hematite is generally the most stable phase of iron oxide [41, 42], with a corundum crystal structure and displays an antiferromagnetic order less than the Néel temperature (955 K). Figure 2.1 (a) shows ferric ions filling 2/3 of the octahedral positions, which are confined by the almost perfect hexagonal close-packed oxygen lattice. It is utilized for the production of pigments, gas sensors, and catalysts because of its cost effectiveness, high corrosion-resistance and its use as precursor for the synthesis of other phases (such as magnetite and maghemite) [43-45].

3.2.1(b) Magnetite (Fe_3O_4)

Magnetite is characterized by an inverse spinel structure with a face centered cubic (fcc) unit cell (8 formula per unit cell) and a lattice parameter (a = 0.839 nm) [46]. The structure of magnetite constitutes 32 oxygen ions (O^{2-}) that are closely

packed in the (111) direction. The chemical composition of magnetite includes both ferrous (Fe^{2+}) and ferric (Fe^{3+}) ions. As illustrated in Figure 2.1(b), the crystal structure of magnetite is composed of octahedral and mixed tetrahedral/octahedral layers stacked along (111) direction. Its structure is expressed as: $Fe^{3+}{}_{(A)}\,(Fe^{2+}Fe^{3+})_{(B)}\,O_4$, where Fe^{3+} ions occupy octahedral sites and bounded by four oxygen atoms, while combined Fe^{2+}/Fe^{3+} ions fill the octahedral sites and is enclosed by six oxygen atoms [47, 48]. It has been reported that Fe^{3+} ions contained in A and B sites are joined antiferromagnetically, while Fe^{2+} ions in the B site add to macroscopic ferromagnetic properties [49]. At room temperature, Fe_3O_4 transforms easily to the maghemite phase.

3.2.1(c) Maghemite (γ-Fe_2O_3)

Maghemite can be synthesized via a cost-effective technique with good dispersivity in aqueous media. It is categorized as a ferrimagnetic oxide, and is characterized by a spinel structure similar to that of magnetite (Fe_3O_4) [46]. In contrast to Fe_3O_4 structure, maghemite has a vacancy of divalent iron in its structure; thus, its constituents include trivalent iron (Fe^{3+}) and oxygen ions (O^{2-}). The structure of maghemite can be expressed as: γ-Fe_2O_3: 0.75 $(Fe^{3+})_A(Fe^{3+}_{5/3}\,V_{1/3})_B\,O_4$, where V denotes vacancy of the Fe^{2+}, which is confirmed to be in the octahedral positions [50]. As shown in Figure 2.1(c), the unit cell of its cubic crystal structure comprises 32 oxygen ions (O^{2-}), 21⅓ Fe^{3+} ions and 2⅓ ionic vacancies. It is reported that oxygen anions constitute a compact cubic-shaped arrangement, whereas the distribution of Fe^{3+} ions is asymmetrical between tetrahedral and octahedral sites. Therefore, maghemite is considered a completely oxidized magnetite, and is typified as an n-type semiconductor with a bandgap of 2.0 eV.

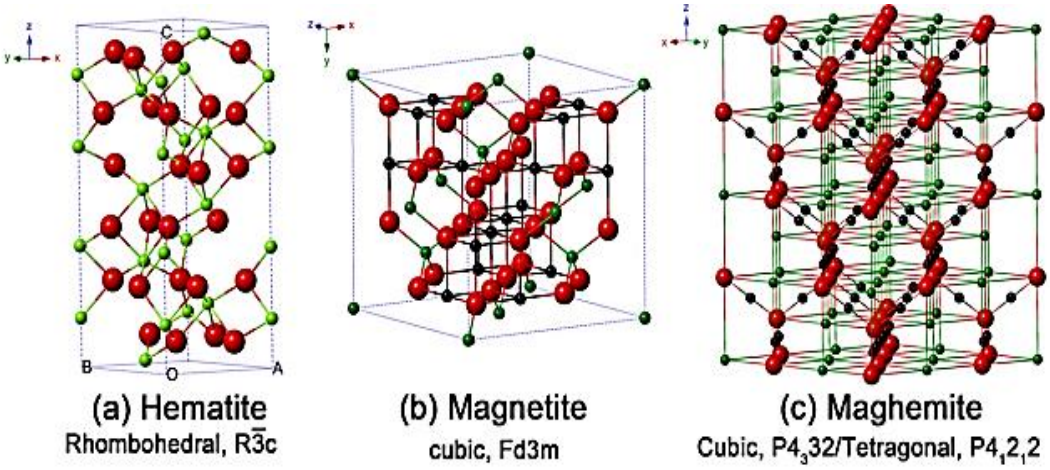

Figure 2.1 Crystal and structure for (a) the hematite, (b) magnetite and (C) maghemite (the red ball is O^{2-}, the green ball is Fe^{3+} and the black ball is Fe^{2+}) (adopted from [16]).

2.2.2 Properties of Iron Oxide Nanoparticles

Iron atoms typically have a large magnetic moment, which is attributable to their four unpaired electrons in the 3d orbital. This magnetic moment arises due to the interactions between the spin and orbital moments of the electron. In the 3d orbital of iron atom, Fe^{3+} and Fe^{2+} comprises five and four unpaired electrons, respectively. At temperatures below the transition temperature, Fe^{3+} and Fe^{2+} may be subjected to phase transitions to a magnetically ordered state and become either ferromagnetic, ferrimagnetic, antiferromagnetic or superparamagnetic [51].

The magnetism of materials depends on their response and alignment to externally applied magnetic field. The magnetism of materials can be classified into: diamagnetic, paramagnetic and ferromagnetic, while ferrimagnetic and antiferromagnetic are considered as subclasses of ferromagnetic [52]. Diamagnetic is a distinctive type of material magnetism that is only created when subjected to an externally applied magnetic field. In a non-magnetic environment, the net magnetization value is zero (no magnetic dipoles). Conversely, in the presence of an externally applied magnetic field, the magnetic dipoles of

diamagnetic materials are pointed reversely to the route of magnetic field. For this reason, magnetic susceptibility of a diamagnetic substance is negative and smaller (-10^{-6}) [53].

For the paramagnetic state, paramagnetic materials are characterized by unpaired electrons, which can be represented as a small magnet with an intrinsic magnetic moment. The dipole moments are randomly aligned; hence there is no net magnetization when the applied magnetic field is removed. In contrast, all magnetic dipoles become uniformly oriented or aligned in the same direction as an applied magnetic field.

Ferromagnetic materials have permanent magnetic moments when there is no externally applied magnetic field. This permanent magnetism behaviour in ferromagnetic substances can be attributed to the uncancelled electron spins in their electron structure. Then again, materials with diverse strengths of magnetic moments that are aligned in anti-parallel manner and generate net magnetization also exhibit ferromagnetic. In the case of antiferromagnetic, the externally applied magnetic field causes magnetic moments in materials arise from an antiparallel alignment, indicating the net magnetization of the material is zero.

However, ferrimagnetic and ferromagnetic nanoparticles display superparamagnetic behaviour. More notably, the magnetic anisotropy of superparamagnetic materials denotes predisposition for the alignment direction of magnetization. Thus, SPIONs randomly flip to the direction of their magnetization. The positioning of superparamagnetic materials in the magnetic field causes their magnetic moments to be oriented parallel to the direction of magnetic field, as a single giant magnetic field [54]. Figure 2.2 shows the classification of magnetism materials by using a plot M vs. H.

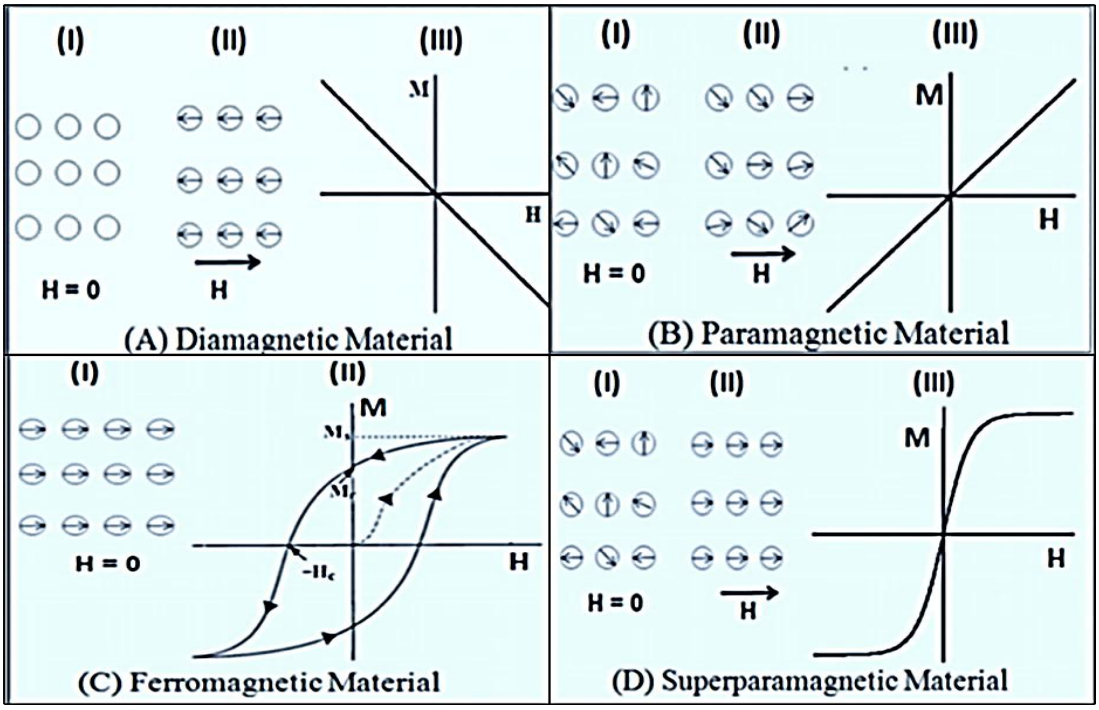

Figure 2.2 Magnetization as a function of the applied magnetic field for diamagnetic material (A), paramagnetic material (B), ferromagnetic material (C), superparamagnetic material (d) (adopted from [55]).

Figure 2.2 shows the material is magnetized when positioned in an external magnetic field (H). Magnetization of material (M) is directly proportional to the strength of magnetic field (H). With increasing H, the M value simultaneously increases until saturation magnetization (Ms) is attained. As the externally applied magnetic field is removed, the material will remain to be magnetized (nonzero magnetization), a phenomenon referred to as remnant magnetization (Mr). To achieve zero magnetization, a coercivity field (Hc) must be applied antiparallel to the magnetic field (H). This relation between coercivity field (Hc) and magnetic field (H) is referred to a hysteresis loop. As crystal particle size decrease, the domains number will concomitantly decrease, resulting in a single domain at below critical value of crystal size. This suggests that the crystal has no hysteresis loop, i.e., it is superparamagnetic, which indicates it has zero magnetization (M=0) when the applied is magnetic field

removed. At room temperature, Iron oxide nanoparticles with sizes below 30 nm often exhibit superparamagnetic behaviour [13].

2.3 Theory of Magnetic Resonance Imaging (MRI)

Magnetic resonance imaging (MRI) is a non-invasive imaging technique that is extensively utilized for clinical diagnosis and studies. MRI has the possibility to scan human body (soft tissue) in 3D at high resolutions. MRI generates images via the measurement of RF signals derived from the magnetic moments of lipid and predominantly H_2O protons contained in biological tissues [56]. As depicted in Figure 2.3, the components of the MR system include: 1) a strong magnet that produces a high magnetic field (B_0), 2) shim coils that form the B_0 as homogeneously as possible, 3) a radiofrequency (RF) coil for the transmission of a radio signal into the tissue or glands being imaged, 4) a receiver coil to detect the returning or reflected radio signals, 5) gradient coils to spatially localize the radio signals, and 6) a computer equipped to reconstruct and ultimately transform the radio signals into the desired image.

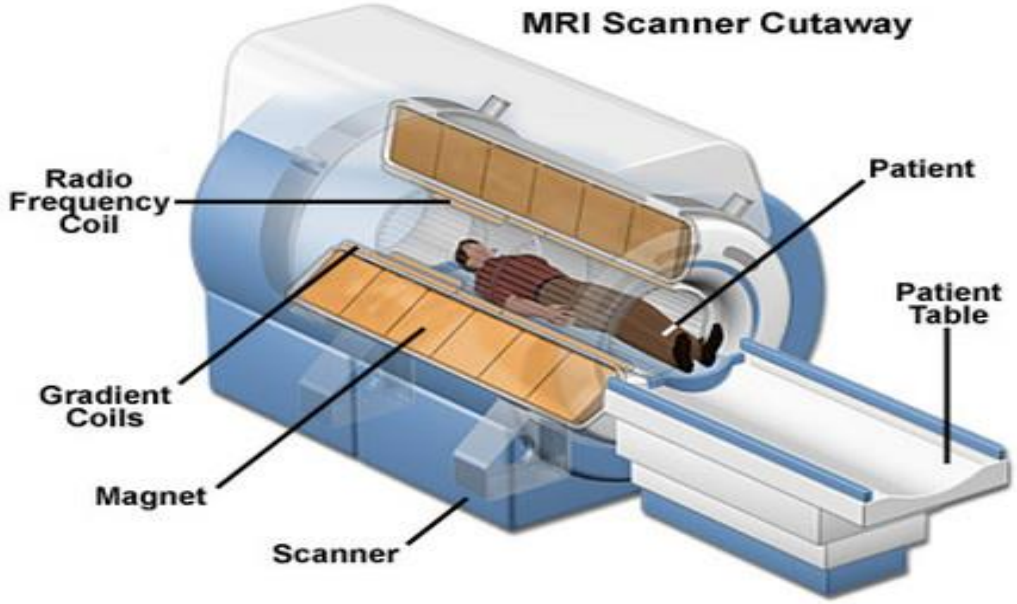

Figure 2.3 Illustration of MRI components [57].

The theory of MRI was developed according to the directional B_0 or moment, which is related to charged nucleons in motion. Atomic nucleus containing protons (positively charged) and neutrons (uncharged) have a specific motion referred to as precession, which generates a small magnetic moment (m) due to the existing charges in the nucleus.

The human body largely comprises H_2O (estimated at 70%), thus, hydrogen nuclei are ubiquitous in body tissue in the forms of water, fat, protein and macromolecules. When a human body is put in a high external B_0, most of the ^1H nuclei become aligned in the direction of the external B_0. The ^1H nuclei precess around the B_0 direction like gyroscopes. This behaviour is referred to as Larmor precession. The nuclei precess with a frequency, denoted as Larmor frequency(ω_0), is proportional to the strength of external magnetic field. The Larmor frequency(ω_0) is expressed in Eq. (3.1) below:

$$\omega_0 = \gamma B_0 \qquad (3.1)$$

where γ symbolizes gyromagnetic ratio (42.58 MHz Tesla^{-1} for ^1H nuclei), and B_0 denotes the external magnetic field. In MRI scan, the value of B_0 generally varies between 0.5 and 1.5 Tesla. At 1.5 Tesla, the Larmor frequency for ^1H nucleus is 63.9 MHz. Therefore, to generate an MRI image of a human body, the body is positioned in a uniform B_0 with values ranging from 0.5 to 1.5 Tesla. The body's ^1H nuclei aligns with the B_0 to produce a net magnetic moment, M, which is parallel to B_0, as illustrated in Figure 2.4.

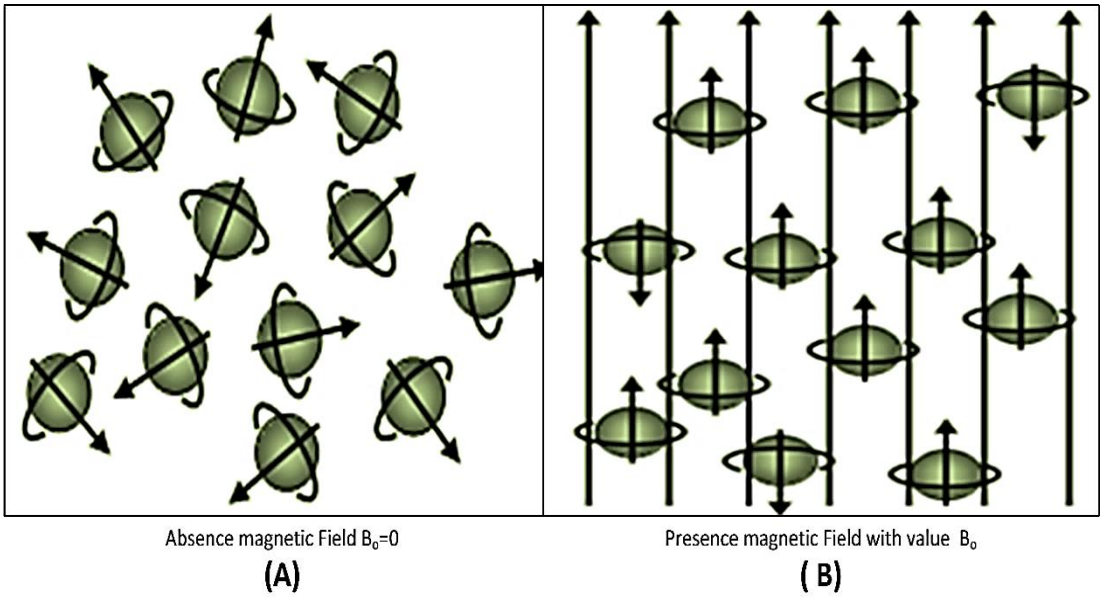

Figure 2.4 Illustration of hydrogen nuclei with magnetic interaction (a) no external magnetic field $B_0 = 0$ (b) presence of external magnetic field B_0 [58]

In a case where a radio wave is applied vertical to the magnetic field, the magnetic vector (M) of ^{1}H proton becomes slanted away from B_0. The radio wave frequency (RF) that initiates the resonance of the ^{1}H proton is reliant on the element of interest (hydrogen) and the strength of the magnetic field.

The strength of the magnetic field can be entirely changed from head to toe by electronic of a sequence of gradient electric coils. By modifying the discrete magnetic field using minute increases, diverse body slices will resonate as various frequencies are applied. As schematically illustrated in Figure 2.5, when M (hydrogen proton) aligns with B_0, a radio-frequency (RF) pulse with Larmor frequency value is introduced perpendicular to B_0. The excitation of proton nuclei into the high-energy state is initiated by this RF pulse. The whole M slants away from B_0 (M_z orientation) with a flip angle α to M_{xy} axis. The longer the duration of applied RF pulse, the higher the intensity and larger the magnitude of the deflection of M as well as higher angle α (90 or 180 degrees).

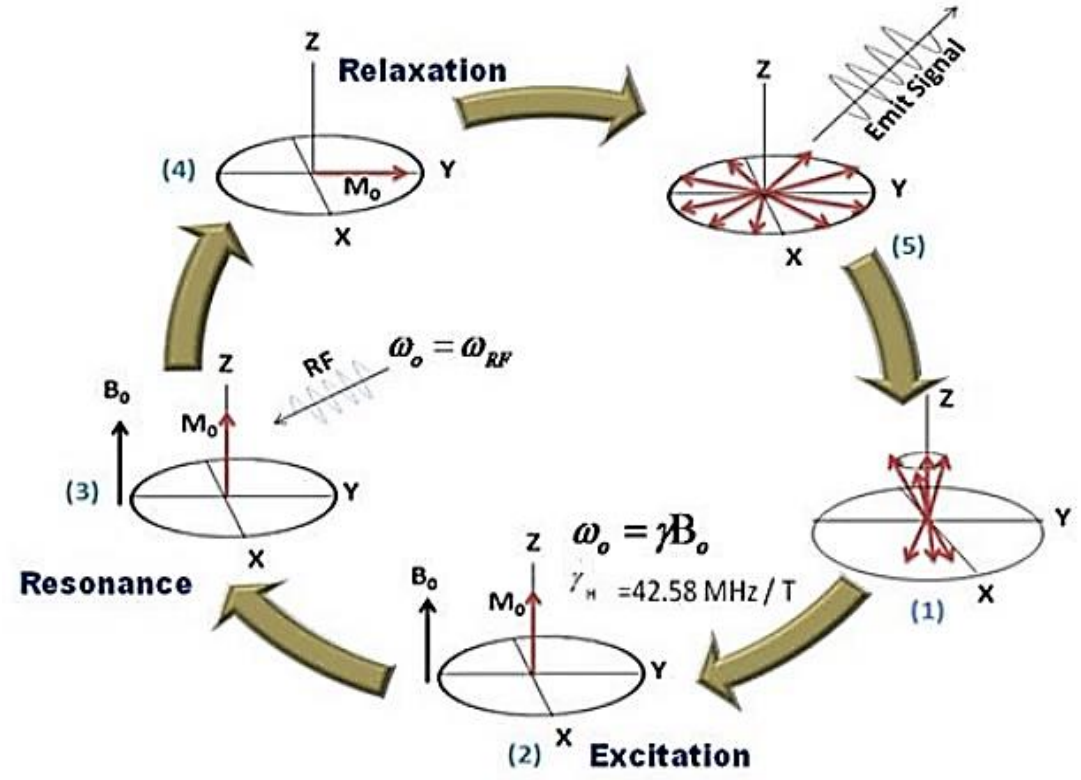

Figure 2.5 Schematic illustration of relaxation procedure in the MRI. (1) The proton nuclei precess randomly (2) The total magnetic moment M of the spin aligns parallel to the external magnetic field. (3) A pulsed RF is introduced and (4) consequently, M flip away from B to the XY plane. (5) When RF is tuned off, the spin diphase at a T_2 decay time and releases their absorbed energy, which is absorbed as MRI signal [59].

The turning-off of the source of radio-frequency causes a reversal of the magnetic vector to its resting state, which initiates the emission of a signal (also a radio wave). This emitted signal is then utilized to produce the MR images. Receiver coils are wound round the target organ to serve as aerials to enhance emitted signal detection. The intensity of the received signal is subsequently plotted on a grey scale or histogram and cross-sectional images are constructed. Multiple transmitted RF pulses can be applied in series to highlight specific organs, tissues or defects. The fact that different tissues display different relaxation rates after turning off the transmitted RF pulse has also been highlighted. The duration required for protons to achieve complete relaxation is determined by measuring the time spin for the reversal of a

magnetic vector to its initial maximum value in the direction of B_o (T_1 relaxation), or the duration for the reversal of axial spin to its resting state (T_2 relaxation).

2.3.1 Relaxation Time (T_1)

The T_1 relaxation time (spin-lattice relaxation time) is the process whereby the net magnetization vector reverts to its initial maximum value in the direction of B_o (resting state). This reverse process of agitated or excited nuclei from the high-energy state to ground state is related to energy loss to adjacent or neighboring nuclei. Nevertheless, T_1 values increase with higher field strengths. Recovery rate is based on T_1, which is distinctive for each tissue. The differential M_z recovery rates for body tissue allow MRI to distinguish various kinds of tissue. T_1 relaxation is an exponential progression, as illustrated in Figure 2.6 (a).

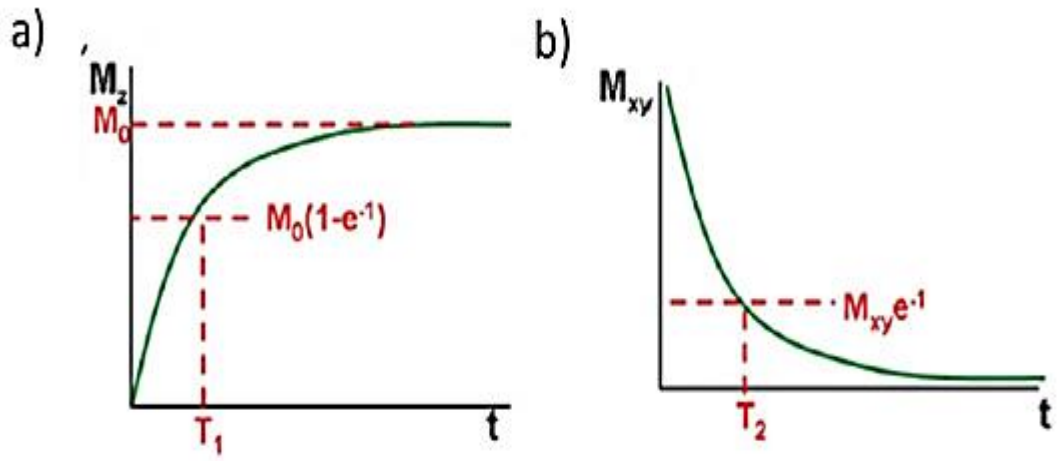

Figure 2.6 This diagram illustrates the simultaneous magnetization of (a) T_1 relaxation and (b) T_2 relaxation after the RF pulse is turned off [60].

The length of the net magnetization vector for a spin echo sequence is specified by Eq. (3.2):

$$M_t(t) = M_0(1 - e^{\frac{-t}{T_1}}) \qquad (3.2)$$

where M_t denotes the magnetization recorded at time t, t indicates the period following the 90^o pulse, M_0 represents the maximum magnetization attained at complete recovery. For t = 1 T_1, the signal reverts to 63% of its original value following the applied of RF pulse. After applying the RF pulse, the magnetization reaches 86% and 95% of its initial value at t= $2T_1$ and $3T_1$, respectively. Thus, spins are regarded as fully relaxed after 3-5 T_1 times.

2.3.2 Relaxation Time (T_2)

T_2 relaxation is defined as the gradual dephasing of spinning dipoles after applying the 90° RF pulse, as observed in a spin-echo order, because of tissue-specific features that influence the rate of movement of protons, majority of which exist in H_2O molecules. T_2 relaxation is also referred to as spin-spin relaxation. This spin-spin relaxation time T_2, is defined as an exponential function by the underlying Eq. (3.3):

$$M_t = M_0 e^{\frac{-t}{T_2}} \qquad (3.3)$$

where M_t represents the quantity of magnetization that decays at time t, while M_o denotes the initial net magnetization. The M_t element of the magnetic vector is subjected to an exponential decline as a function of the time constant (T_2). The exponential decline in the signal from T_2 relaxation is shown in Figure 2.6 (b).

The duration of relaxation time (T_2) in pure water is lengthy, around 3-4 s since H_2O molecules travel at considerably faster rate than the Larmor frequency. The fast movement leads to the equivalence of T_1 and T_2 in pure water. The relaxation rate is much faster in solutions of macromolecules and tissues, i.e., the T_2 time is relatively shorter, partly due to the sluggish or slower motion of protons both in macromolecules and intrinsically adsorbed H_2O molecules. This relatively slower motion is nearer to

the Larmor frequency. Cases of T_1 and T_2 in living tissues are: T_1=1.9 s and T_2=0.25 s in cerebrospinal fluid, and T_1=0.5 s and T_2=0.07 s in brain white matter.

Therefore, movement and the local field variations reduce below the Larmor frequency in biological cells and ligaments, dipoles that are aligned with the main magnetic field start contributing to T_2 relaxation by causing local variations in precession rate. The resultant short T_2 time leads to dark appearances denoting tendons and other semi-solid tissues in T_2-weighted images, while lengthy duration T_2 fluids with small volume of macromolecules such as H_2O, urine and cerebrospinal fluid will look bright on T_2-weighted images. The loss of signal and darkness in T_2-weighted images in cortical bone, teeth, and calculi are mainly due to the presence of relatively small amounts of H_2O (low proton density) in contrast to softer tissues such as tendons and ligaments. H_2O contained in bone, teeth and calculi are typically adsorbed in collagen, thus are characterized by a very short T_2 time and exhibit dark appearances. In addition, there are minor susceptibility variances between bone and soft tissue, which account for the dark appearance at boundaries between marrow and bone trabecula, which is specifically observed on gradient echo images.

2.4 MRI Contrast Agent

The disparity in signal intensity between adjacent tissues in an image is referred to as tissue contrast [61]. In MRI, the natural contrast depends on certain parameters, which include spinning proton density, and signal intensities on T_1 and T_2 [62]. Spinning proton density is defined proton concentration in human tissue, existing as H_2O molecules and macromolecules (proteins, carbohydrates, fat, etc). The T_1 and T_2 relaxation times describe the mechanisms by which the protons revert to their inert states, following the originally applied RF pulse. As observed in Figure 2.7, combining MRI with contrast agents (Gadolinium) significantly enhances the depiction of

inflamed tissues such as in tumor angiogenesis [63-65], atherosclerotic plaques [66, 67], arthritis [68], and the disintegration of the blood brain barrier associated with pathologies, for example, multiple sclerosis [69].

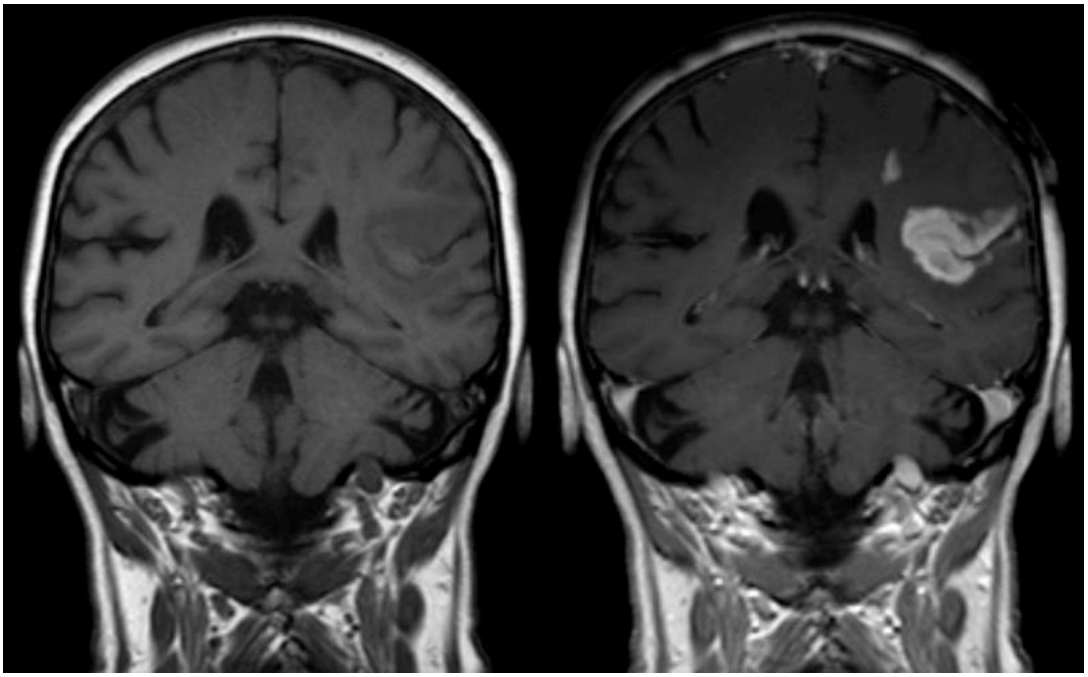

Figure 2.7 Comparing MRI with and without contrast agents (Gadolinium). Left image is without contrast agent. Right image is with contrast agent (Gadolinium) [70].

Differences in MRI image contrast can be altered through adjusting both pulse sequences and image parameters. A pulse sequence controls the gradient pulses, timing of the RF, strength, and specific number. The repetition time (TR) and the echo time (TE) are the most important factors. The repetition time (TR) is the time between successive 90^0 RF pulse. The echo time (TE) is the duration between the original 90^0 RF pulse and the echo, as shown in Figure 2.8. The repetition time (TR) and the echo time (TE) are pulse sequence parameters which are adjusted to modify the MRI contrast.

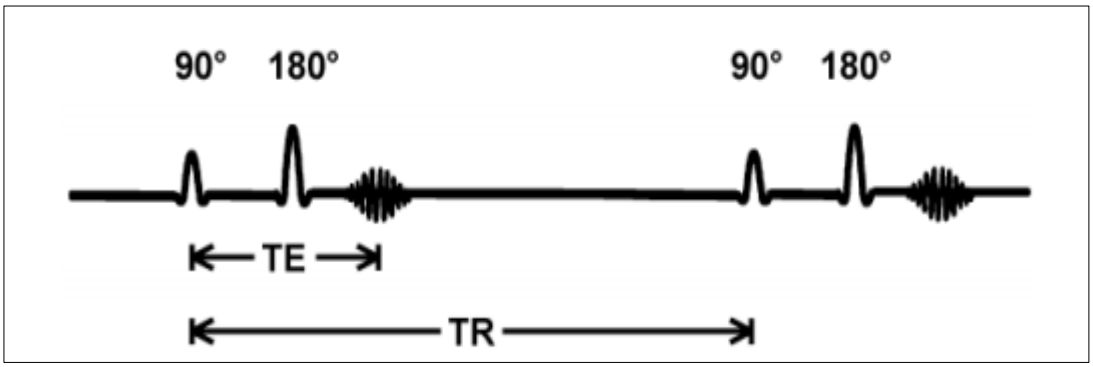

Figure 2.8 Schematic representation of TE and TR [59].

MRI can't always show the difference between unhealthy tissues and the healthy tissue, which means using MRI contrast agent may be needed. It is recognized that gadolinium ions (Gd^{3+}) and superparamagnetic iron oxide nanoparticles (SPIONs) are the generally utilized contrast agents due to their effective T_1 and T_2 relaxation times of ^1H, respectively. However, gadolinium-based contrast agents have several drawbacks, which include their high toxicity, short lifecycle, and poor cellular uptake [13]. Conversely, the applicability of SPIONs as potential materials for *in vivo* MRI contrast is based on their high signal sensitivity and fast detectability by means of electron microscopy [17, 71]. Therefore, one of the main objectives of this research is to examine the use of SPION as MRI T_2 contrast agent by using Agarose gel phantom. Agarose gel is a promising material for constructing MRI phantom, as it does not require refrigeration, resists melting and spoilage, and may be reused. Agarose gel phantoms provide images similar to real tissue [72]. The performance of the SPION nanoparticles in Agarose gel phantom as MRI contrast agent will be discussed in Section 4.7.

2.5 Summary

In this chapter, the various iron oxide phases and their crystal structure were presented. The classification of materials magnetism was discussed, depending on their response and alignment to externally applied magnetic field. The magnetism of

materials was classified into: diamagnetic, paramagnetic and ferromagnetic, while ferrimagnetic and antiferromagnetic are considered as subclasses of ferromagnetic. The theoretical background on MRI and MRI contrast agent were also explained in this chapter. The use of gadolinium ions (Gd^{3+}) and superparamagnetic iron oxide nanoparticles (SPIONs) as MRI contrast agents was discussed. The main advantages of using agarose gel in preparation MRI phantoms were explained.

CHAPTER 3: LITERATURE REVIEW

3.1 Brief Overview of Iron Oxide Nanoparticles

In recent times, the interest of researchers in the synthesis and improving potential applications of iron oxide nanoparticles (IONPs) has increased tremendously on account of their physicochemical and magnetic properties [73]. IONPs have quite a few characteristic phases such as magnetite (Fe_3O_4), hematite (α-Fe_2O_3), maghemite (γ-Fe_2O_3), and goethite (FeO(OH)) [39]. The superparamagnetic behaviour, biocompatibility, and low toxic nature of magnetite and maghemite make them the most utilized phases for biomedical applications [35, 36]. Furthermore, this research focused only on the superparamagnetic behaviour of IONPs and their surface modification with different surfactants.

3.2 Synthesis of Iron Oxide Nanoparticles

To synthesize of SPIONs, several techniques such as thermal decomposition, microemulsion, electrochemical, solvothermal, sol-gel, sonochemical and co-precipitation method have been used. The co-precipitation technique is the simplest and most cited approach for the preparation of SPIONs. The underlying section presents and discusses the different methods for synthesizing SPIONs in the last decade. These methods synthesize SPIONs, either magnetite or maghemite, by controlling reaction conditions.

3.2.1 Thermal Decomposition Method

Thermal decomposition is the foremost method applied to synthesize highly crystalline and monodispersed SPIONs [37]. This technique involves the use of high temperature to subject organometallic precursors, such as iron (III) acetylacetonate, iron pentacarbonyl and iron fatty acid to decomposition in the presence of solvents or

solvent-free environment with high boiling point (>250 ^{o}C) [74, 75]. However, particle size cannot be controlled in solvent free environment due to surfactant boiling temperature [74]. Different synthesis parameters such as temperature of reaction, type of solvent, concentration of surfactants, and ratio of organic iron precursors/surfactant have been proven to control the physicochemical and magnetic properties of SPIONs [76, 77]. As illustrated in Figure 3.1, Demortière et al. synthesized different sizes of NPs ranging from 2.5 to 14 nm by simply controlling the conditions of thermal decomposition and utilizing several solvents, i.e. din-hexyl ether (2.5 nm) eicosene (14 nm), hexadecene (3.5 nm), di-n-octyl ether (5 nm), dibenzyl ether (9 nm) and di-n-octyl ether (11 nm) [78]. In different study, the use of surfactant (oleic acid) to obtain the narrow size distribution of Fe_3O_4 NPs with a mean particle size of 16 nm [30].

Furthermore, a number of studies have employed the thermal decomposition method to synthesize monodisperse and highly crystalline SPIONs. For instance, Ruusunen et al. produced magnetite nanoparticles by controlling the volume of oxygen in the reactor [79]. Dai et al. used polyethylene glycol (PEG) as a polymer to produce highly water soluble SPIONs in alcoholic solvent via thermal decomposition [80]. Amara et al., prepared varying amounts of ferrocene and polyvinylpyrrolidone (PVP) to yield magnetite nanocubes and nanospheres via thermal decomposition in the absence of a solvent, which is a novel, non-complex and single-step process [81]. Patsula et al. synthesized monodispersed SPIONs via thermal decomposition of Fe^{3+} glucuronate ($Fe(Glu)_3$) in the presence poly(3-Omethacryloyl-α-D-glucopyranose) as a stabilizing agent. The study showed that the morphology of the synthesized structures is dependent on experimental variables that include reaction temperature and concentration of the surfactant in addition to composition of the high-boiling point solvent (hydrocarbons or polyethers) [82]. Orsini et al. investigated the role of heating

rates on the synthesis of SPIONs with diameter range of 7 nm ≤ d ≤ 12 nm, via the degradation of iron(III) acetylacetonate at high temperature [83].

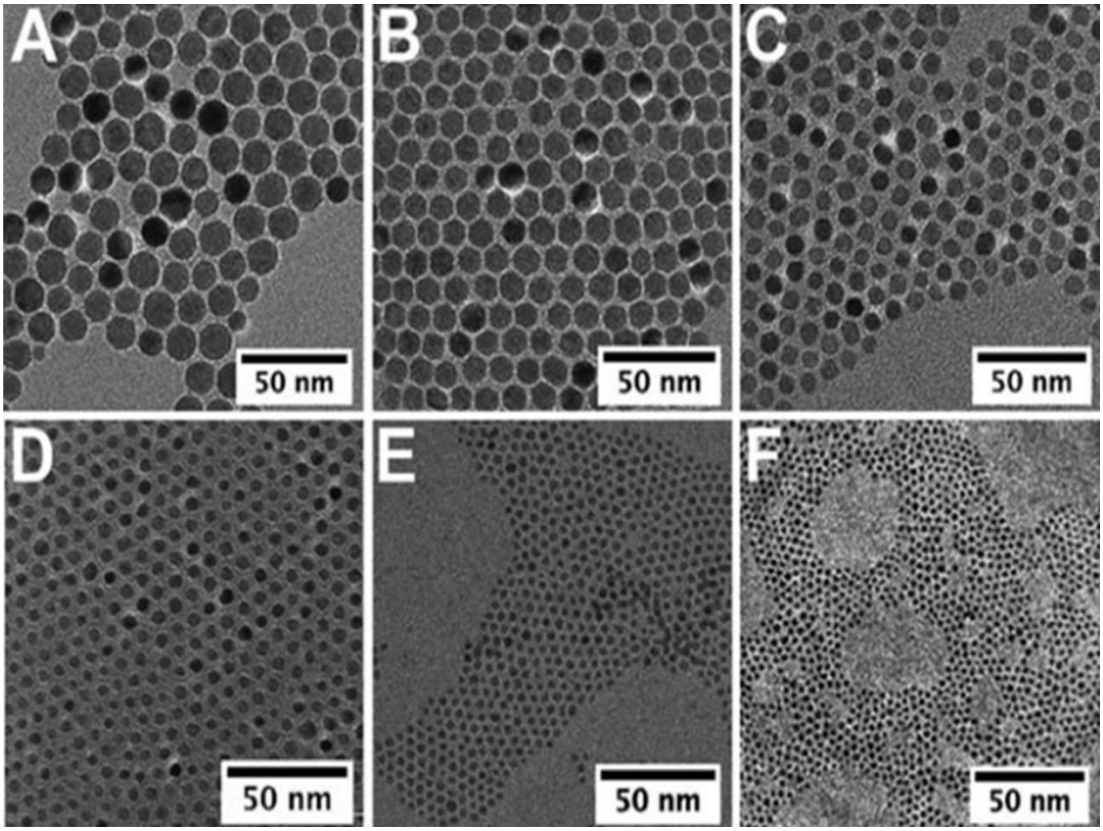

Figure 3.1 TEM images of IONPs prepared in different solvent types of 14 nm (eicosene) (A), 11 nm (di-n-octyl ether) (B), 9 nm (dibenzyl ether) (C), 5 nm (di-n-octyl ether) (D), 3.5 nm (hexadecene) (E), and 2.5 nm (di-n-hexyl ether) (F) (adopted from [78]).

3.2.2 Microemulsion Method

Microemulsion is a mix of immiscible liquids, usually water and oil, which has attained thermodynamic stability [84]. In the presence of surfactants, the immiscible liquids co-occur in one phase with hydrophilic–lipophilic balanced (HLB) properties [85]. The two most frequently used microemulsions to synthesize NPs are Water-in-Oil (W/O) and Oil-in-Water (O/W). However, synthesizing magnetic nanoparticles via the microemulsion process is based on the combination of immiscible liquids, water and oil, containing Fe ions and precipitating agent type, respectively.